Applied Catalysis B: Environmental 220 (2018) 19–30

Contents lists available at ScienceDirect

Applied Catalysis B: Environmental

journal homepage: www.elsevier.com/locate/apcatb

Research paper

Remarkable enhancement of the selective catalytic reduction of NO at low temperature by collaborative effect of ethanol and NH_3 over silver supported catalyst

M. Barreau, M.-L. Tarot, D. Duprez, X. Courtois*, F. Can*

University of Poitiers, CNRS, UMR 7285, Institut de Chimie des Milieux et Matériaux de Poitiers (IC2MP), 4 Rue Michel Brunet, TSA 51106, 86073 Cedex 9, France

ARTICLE INFO

Article history:
Received 13 April 2017
Received in revised form 26 July 2017
Accepted 2 August 2017
Available online 5 August 2017

Keywords:
NOx
SCR
Ethanol
NH_3

ABSTRACT

The NO_x selective catalytic reduction (SCR) is extensively studied as an effective process for air pollutants abatement from lean burn and Diesel vehicles. In the implemented Urea-SCR technology, the NO_2/NO_x ratio is a key parameter that limits the deNO_x efficiency at low temperature (175–250 °C). We demonstrate that co-feeding of ammonia and ethanol on a Ag/Al_2O_3 catalyst enables a drastic enhancement of the NO_x conversion at temperatures below 200 °C using only NO as NO_x (standard SCR condition). Even if NO_2 is provided at low temperature by the NO oxidation over Ag/Al_2O_3 in presence of EtOH, the NO_x conversion improvement is not only due to a direct reaction between NH_3 and NO_x, but mainly attributed to the availability of hydrogen H* species resulting from EtOH oxidation (similar to a H_2 assisted NH_3-SCR process). Due to the presence of remaining NH_3 and NO_2 (formed over Ag/Al_2O_3 catalyst), further deNO_x efficiency improvement was obtained at low temperature by addition of a NH_3-SCR catalyst (WO_3/Ce-Zr). The critical dependence of the SCR process on the Diesel Oxidation Catalyst (DOC) efficiency at low temperature is thus avoided.

1. Introduction

Air pollution is responsible of direct harmful effects on human health with hundred thousand deaths per year throughout the world [1]. Consequently, stringent standards regulate pollutants emissions such as for nitrogen monoxide (NO) and nitrogen dioxide (NO_2) from stationary and mobile sources.

Worldwide, the introduction of three way catalyst (TWC) converters for gasoline spark ignition engines noticeably contributed to increasing the air quality [2–4]. However, for internal combustion engines operated in excess of air, such as Diesel engines, TWC converter is unable to efficiently reduce NO_x into N_2 and the implementation of selective catalytic reduction (SCR) technology, with a large choice of reductants, is described as one of the most promising way to control NO_x emissions in lean media.

Among the various possible reductants, ammonia (or urea used as NH_3 provider), hydrocarbons (propene, propane, decane...), ethanol (EtOH) were widely studied. Interestingly, whatever the considered reductant, the mechanistic studies generally suggest that N_2 is obtained *via* the formation of species like —CN and —NCO, which are known to be involved in ammonia formation. Indeed, such species were identified during the lean NO_x reduction by propene over $LaFe_{1-x}(Cu, Pd)xO_{3-\delta}$ perovskites [5], supported transition metals like $Cu/Ti_{0.7}Zr_{0.3}O_2$ [6], or supported noble metals like Rh/TiO_2 [7]. NH_3 intermediate species was also clearly identified over Cu-ZSM-5 exchanged zeolite when propane [8] or decane [9] are used, as well as during the NO_x reduction process by ethanol over Ag/Al_2O_3 catalyst [10]. These examples point out the key role of the ammonia-like intermediate species in the deNO_x pathway, whatever the considered reductant and the type of catalyst (noble metal, oxide, zeolite...).

To meet the current environmental standards limiting the NO_x emission from Diesel vehicles, the automotive industry has commonly adopted the Urea-SCR technology. The use of an aqueous urea solution as ammonia precursor is a safe and operational adaptation of the NH_3-SCR technology initially developed for stationary sources. Urea (NH_2—CO—NH_2) is theoretically decomposed in ammonia via two consecutives reactions: urea thermal decomposition and HNCO hydrolysis reactions. Thereafter, NO_x reduction is assumed to be correlated with NH_3 yield and supposed to follow

* Corresponding authors.
E-mail addresses: xavier.courtois@univ-poitiers.fr (X. Courtois), fabien.can@univ-poitiers.fr (F. Can).

http://dx.doi.org/10.1016/j.apcatb.2017.08.015
0926-3373/

similar pathways than those demonstrated with ammonia reductant:

$$NO + NO_2 + 2NH_3 \rightarrow 2N_2 + 3H_2O \quad (1)$$

More precisely, the fast-SCR reaction (Eq. (1)) results from sequences involving ammonium nitrate or related surface species as intermediates (Eqs. (2), (3)):

$$2NO_2 + 2NH_3 \rightarrow N_2 + NH_4NO_3 + H_2O \quad (2)$$

$$NO + NH_4NO_3 \rightarrow N_2 + NO_2 + 2H_2O \quad (3)$$

Firstly, ammonium nitrate formation (Eq. (2)) involves NO_2 reactivity by dimerization (Eq. (4)), disproportionation (Eq. (5)), and successive reaction to form N_2 (Eq. (6)) and ammonium nitrate (Eq. (7)). The second step of the fast-SCR chemistry (Eq. (3)) implies the NO reactivity with ammonium nitrate which proceeds via the NO oxidation by nitric acid (Eq. (8)) followed by reaction of NH_3 with nitrous acid to form N_2 (Eq. (6)). As a result, conversion of nitrogen oxides is optimized when NO, NO_2 and NH_3 respect a 1:1:2 ratio, enabling the stoichiometric reaction of fast SCR and is intimately related to HONO/HNO_3 reactional pathway [11,12–15]. Finally, N_2 is obtained by decomposition of ammonium nitrite (Eq. (6)). With many practical catalysts and regardless the used reductant, this reaction is commonly suggested to be the final step of deNO_x chemistry [16,17–19].

$$NO_2 \rightleftarrows N_2O_4 \quad (4)$$

$$N_2O_4 + H_2O \rightleftarrows HONO + HNO_3 \quad (5)$$

$$NH_3 + HONO \rightleftarrows NH_4^+ + NO_2^- \rightleftarrows NH_4NO_2 \rightarrow N_2 + 2H_2O \quad (6)$$

$$NH_3 + HNO_3 \rightleftarrows NH_4^+ + NO_3^- \rightleftarrows NH_4NO_3 \quad (7)$$

$$NO + HNO_3 \rightleftarrows NO_2 + HONO \quad (8)$$

Unfortunately, the on-board Urea-SCR technology suffers from a poor activity at low temperatures (200 °C) due to an insufficient NO_2/NO_x ratio to promote the fast SCR stoichiometry (Eq. (1)) [20]. NO_2 yield can be adjusted by the Diesel oxidation catalyst (DOC) upstream of the SCR converters, but the oxidation activity is also strongly dependent on both temperature and operating conditions. Recently an over-injection of aqueous solution of ammonium nitrate (Eq. (9)) was reported to enhance the deNO_x efficiency while avoiding NO pre-oxidation [11].

$$2NO + 2NH_3 + NH_4NO_3 \rightarrow 3N_2 + 5H_2O \quad (9)$$

EtOH-SCR process was also described as an attractive way to reduce NO_x, especially due to the practicality/availability of ethanol and its relative safety. Silver-based materials were found to be the most active and selective for the NO_x reduction by oxygenates reductant compounds [19,21]. With ethanol as reductant, the NO conversion is assumed to be strongly dependant of the nitromethane route, based on the ethanol oxidation to acetaldehyde via a variety of intermediates which are subsequently adsorbed, such as surface acetate and ethoxide ions leading to the global reaction (Eq. (10)):

$$C_2H_5OH + 6NO \rightarrow 3N_2 + 2CO_2 + 3H_2O \quad (10)$$

N-containing compounds as HNCO and ammonia are also eventually produced [10,22–26] as surface organic intermediate. A detailed surface mechanism for the SCR of NO_x with ethanol on silver alumina catalyst was proposed by Tham et al. [24]. In summary, the first step of the reaction framework results in C_2H_5OH dissociative adsorption into surface ethoxide $C_2H_5O^*$ and surface hydrogen H^* ad-species (Eq. (11)) [26]. Thereafter, ethoxide can be consumed either by the oxidation pathway to yield acetaldehyde (Eq. (12)) or by the NO_x reduction pathway via nitromethane route (Eqs. (13)–(16)).

$$C_2H_5OH \rightarrow C_2H_5O^*_{(ad)} + H^*_{(ad)} \quad (11)$$

$$C_2H_5O^*_{(ad)} \rightarrow CH_3CHO^*_{(ad)} + H^*_{(ad)} \rightarrow CH_3CHO \quad (12)$$

$$CH_3CHO^*_{(ad)} + O^*_{(ad)} \rightarrow CH_3COO^*_{(ad)} + H^*_{(ad)} \rightarrow CH_3COOH \quad (13)$$

$$CH_3COO^*_{(ad)} + NO_2 \rightarrow CH_3NO_2 + CO_2 \quad (14)$$

$$CH_3NO_2 \rightarrow HNCO + H_2O \quad (15)$$

$$HNCO + H_2O \rightarrow NH_3 + CO_2 \quad (16)$$

Interestingly, the formation of ammonia *via* the isocyanate hydrolysis route (Eq. (9)) takes place in this reaction pathway. It is assumed that the reaction pathway then follows very similar routes to those reported for the NH_3-SCR reaction, with N_2 formation from ammonium nitrite decomposition (Eq. (6)).

Unfortunately, the deNO_x activity of the EtOH-SCR technology at low temperatures appears not sufficient for a practical application to the next generation of the energy-efficient Diesel vehicles, especially due to the rate limiting step of CH_3NO_2 formation at T < 250–300 °C. However, some studies reported that an improvement of NO_x reduction efficiency of EtOH-SCR technology at low temperature is possible. For instance, addition of hydrogen into the reaction mixture allows an enhancement of the deNO_x efficiency. It was advanced that H_2 addition promotes the partial oxidation of C_2H_5OH to form enolic species which mainly contribute to accelerate NO_x reduction [27–29]. Note that Ag/Al_2O_3 catalysts were reported to exhibit a poor activity in NH_3-SCR but they become very active in case of H_2 addition [30–32]. An improvement of the N_2 yield can also be obtained modifying the alumina support to form surface zinc aluminates [21]. Indeed, an activation of the ethanol conversion in acetaldehyde was observed, but mainly from 250 to 300 °C.

Interestingly, the ethanol dehydrogenation leading to acetaldehyde appears concomitant with a high proportion of NO_2 emission from NO oxidation, as previously reported by Flura et al. [23]. This NO_2 formation at relatively low temperature (from 150 °C) may also favourably interfere in the SCR process, favouring the fast SCR reaction (Eq. (1)). Moreover, the formation of ammonia by the isocyanate hydrolysis route (Eq. (9)) appears in the EtOH-SCR reaction pathway. Ammonia was detected for temperature higher than 250 °C, when NO_x reach a high conversion level [23]. It could indicates that ammonia is a key intermediate species, but with a too low production rate at low temperature.

Obviously, N_2 yield of EtOH-SCR process seems to appear strongly dependant to subsequent ammonia route formation. Thus, in the present work, we studied the role of ammonia as co-reactant species for assisted EtOH-SCR process in NO rich media for future application in a coupled Urea/Ethanol-SCR process. Particular attention was paid to increasing the efficiency of EtOH-SCR system at low temperatures (T = 175–250 °C) while overcoming the NO_2 yield of the DOC.

2. Experimental part

2.1. Materials

Silver supported catalyst was selected to conduct EtOH-SCR experiments due to their high reactivity toward oxygenated compounds [33–35]. Alumina support was provided by Axens and exhibited a specific surface area of 170 $m^2\,g^{-1}$ after calcination 4 h under air at 700 °C. Silver (2.0 $_{wt.}$%, which is commonly described as the optimal loading [36]) was added by impregnation of $AgNO_3$ dissolved in ethanol [21,23,37]. Sample was finally calcined under synthetic air with 10% H_2O at 700 °C for 4 h and is noted Ag/Al.

$WO_3/Ce_xZr_{1-x}O_2$ catalyst was selected as NH_3-SCR material [38–40]. Ceria-zirconia support (40_{wt}% of CeO_2) was provided by Solvay. This solid solution, was first calcined 4 h under air at 700 °C before use and exhibited a specific surface area of 73 $m^2\,g^{-1}$. Tungsten (6_{wt}% WO_3) was added by impregnation at 60 °C under continuous agitation using an aqueous solution of ammonium metatungstate. After drying at 80 °C, the preparation was placed in an oven at 120 °C during a night. Finally, the solid was calcined under synthetic wet air (10% H_2O) during 4 h at 700 °C. The obtained catalyst is noted WO_3/Ce-Zr.

2.2. Characterization

Specific surface areas were determined by BET method (Tristar 3000, Micromeritics) using nitrogen adsorption at 77 K. Prior to the N_2 physisorption, the samples were degassed under vacuum 2 h at 250 °C. The Ag/Al and WO_3/Ce-Zr catalysts exhibited specific surface areas of 160 and 52 $m^2\,g^{-1}$, respectively.

The powder XRD patterns of Ag/Al was collected using an Empyrean (PANalytical) diffractometer. Data acquisition was recorded from 20° to 120° (2θ) with a scanning step of 0.1°. X-ray diffraction pattern evidenced the γ-Al_2O_3 phase [ICDD PDF n° 00-050-0741(I)] with no visible reflection assigned to silver species (Ag^0, Ag_2O, AgO, $Ag_2Al_2O_4$...).

Temperature programmed reduction (TPR) experiments were performed on a Micromeritics Autochem 2920 apparatus equipped with a thermal conductivity detector (TCD). Sample of about 100 mg was placed in a U-shape quartz reactor. Prior to the TPR measurements, the sample was calcined at 500 °C for 60 min under O_2 flow (heating rate: 5 °C min^{-1}). The sample was cooled down to room temperature, and it was purged under Ar flow for 45 min. The reduction was carried out under 1 vol.% H_2 in Ar flow up to 500 °C (heating rate: 5 °C min^{-1}). TCD signal being sensible to water, an H_2O-trap was added downstream of the reactor, allowing the quantification of the H_2 consumption during the TPR experiment. H_2-TPR experiment of Ag/Al showed a broad H_2 consumption peak, with a maximum at around 260 °C. Hydrogen consumption indicated that 33% of the deposited silver was in metallic state, according to results previously reported by Musi et al. [41].

Transmission Electron Microscopy (TEM) micrographs were recorded on JEOL 2100 instrument (operated at 200 kV with a LaB_6 source and equipped with a Gatan Ultra scan camera). TEM experiments showed that Ag/Al_2O_3 presents small silver particles, most of the particles ranging below 3 nm (Supplementary information (SI) file, Fig. S1).

Infrared characterization was carried out with a Nicolet 6700 infrared spectrometer equipped with a MCT detector and a KBr beamsplitter using a resolution of 4 cm^{-1} and 126 scans. A home-made designed cell (SI file, Fig. S2) that allows *in situ* treatment and high temperature adsorption of probe molecule was used. The cell was connected to a vacuum manifold system which could supply nitric oxide, ethanol, ammonia and oxygen. Silver supported catalyst was pressed as self-supported wafer (disc of about 20 mg, 2 cm^2) and was firstly treated *in situ* at 400 °C under vacuum (residual pressure of about 5×10^{-5} hPa). The calibrated doses of desired gas mixture were successively added at 200 °C up to equilibrium pressure. Three gas mixtures (EtOH-O_2, NO-O_2 and NH_3) and combinations of co-adsorption (EtOH-O_2 + NH_3, NO-O_2 + NH_3, EtOH-O_2 + NO-O_2 + NH_3) were particularly studied. For EtOH-O_2 and NO-O_2 mixtures, the O_2/reductant pressure ratio was fixed at 5. The spectra presented in this paper were normalized to a disc of 10 mg cm^{-2} and the reference spectra (recorded at 200 °C after calcination) was systematically subtracted to highlight the adsorbed species.

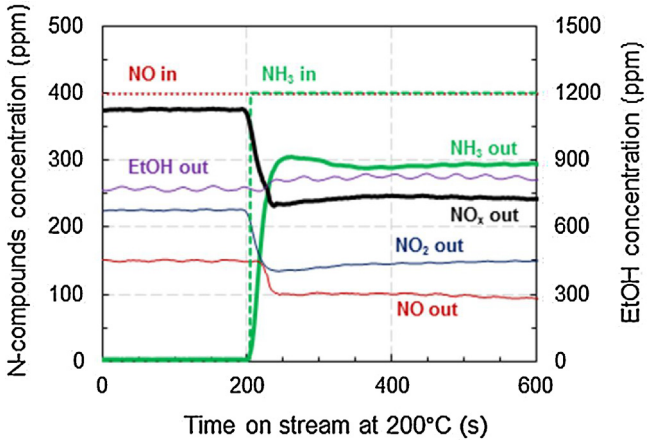

Fig. 1. Effect of NH_3 co-feeding (400 ppm) at 200 °C on NO_x (NO, NO_2), C_2H_5OH, and NH_3 outlet concentrations over Ag/Al in EtOH-SCR (400 ppm NO, 1200 ppm C_2H_5OH, 8% H_2O, 10% CO_2, 10% O_2 balanced in N_2).

2.3. Catalytic tests

Catalytic tests were performed in a quartz tubular micro-reactor under a synthetic flow simulating a realistic Diesel engine exhaust. The total flow rate was fixed at 333 mL min^{-1} for 100 mg of powdered catalyst diluted in 100 mg SiC, both sieved between 100 μm and 250 μm, corresponding to a GHSV of 130,000 h^{-1} toward the catalyst (200 L h^{-1} $g_{cata}{}^{-1}$; 100 L h^{-1} $g_{powder}{}^{-1}$). For the dual-bed configuration, 100 mg of WO_3/Ce-Zr were placed downstream 100 mg of Ag/Al catalyst (no SiC for these experiments).

Three reductants were evaluated, namely ethanol (EtOH), NH_3, and a blend (EtOH + NH_3). The compositions of the gas mixtures for the various catalytic tests are reported in Table 1. Gaseous $NO/NO_2/NH_3/O_2/N_2$ gas flows were adjusted by mass-flow controllers (Bronkhorst). Ethanol aqueous solution (8.02×10^{-1} mol L^{-1}) was vaporized and mixed upstream the SCR catalyst by means of a micro-nozzles provided by The Lee Company ($Ø_{nozzle}$ = 50 μm) connected to a HPLC pump (Jasco, PU-2085, 22 μL min^{-1}, ΔP = 10 bar). The compositions of the feed gas and effluent stream were monitored continuously using online MKS 2030 Multigas infrared analyser for NO, NO_2, N_2O, HNCO, NH_3, CH_3CH_2OH, CH_3CHO, CH_3OH, CH_2O, C_2H_4, CH_4, CO, CO_2 and H_2O.

3. Results and discussion

The NO reduction by ethanol (EtOH-SCR condition, Table 1) over Ag/Al catalyst is the reference test in this study. EtOH and NO concentrations were fixed at 1200 ppm and 400 ppm respectively, corresponding to a usual C/N ratio of 6 [10,21,23]. First, note that N_2O emissions were limited at a very low level whatever the involved catalytic system. More precisely, N_2O was detected with a maximum concentration of 6 ppm from 250 to 500 °C in EtOH-SCR condition. The maximum N_2O concentration (11 ppm) was recorded at 450 °C over Ag/Al catalyst in (EtOH + NH_3)-SCR condition.

3.1. Highlight of the (EtOH + NH_3) collaborative effect on NO SCR

To highlight the beneficial effect of (EtOH + NH_3) co-feeding on the NO reduction rate over Ag/Al, Fig. 1 reports the evolution of outlet gas feed composition *versus* time on stream for NO, NO_2, C_2H_5OH, and NH_3 over Ag/Al catalyst at 200 °C, before and after NH_3 co-addition. With only ethanol as reductant (EtOH-SCR condition), NO_x conversion reached 9% and a significant NO_2 outlet concentration was recorded at 225 ppm, which corresponds to a NO_2/NO_x

Table 1
Composition of the Gas mixtures of the SCR tests (total rate: 333 mL min^{-1} for 100 mg of powdered catalyst).

Catalytic test	NO (ppm)	NO_2 (ppm)	NH_3 (ppm)	C_2H_5OH (ppm)	H_2 (ppm)	O_2 (%)	CO_2 (%)	H_2O (%)	N_2
Standard-NH_3-SCR	400		400			10	10	8	balance
Fast-NH_3-SCR	200	200	400			10	10	8	
EtOH-SCR	400			1200		10	10	8	
(EtOH + NH_3)-SCR	400		400	1200		10	10	8	
H_2-SCR	400				400	10	10	8	

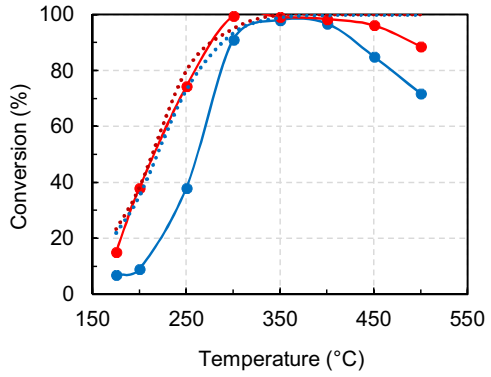

Fig. 2. Comparison of EtOH-SCR (blue) and (EtOH + NH_3)-SCR (red) behaviour in NO_x conversion (full line) and EtOH conversion (dotted line) over Ag/Al catalyst. (For interpretation of the references to color in this figure legend, the reader is referred to the web version of this article.)

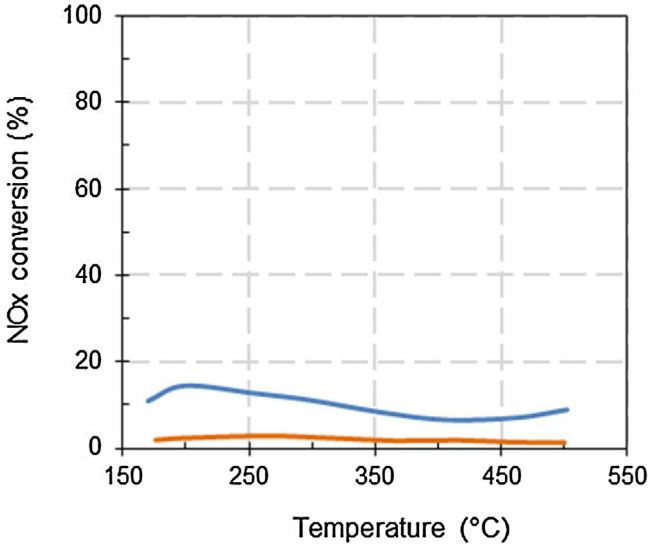

Fig. 3. NO_x conversion in NH_3-SCR over Ag/Al catalyst for standard-SCR condition (▬: 400 ppm NO, 400 ppm NH_3, 8% H_2O, 10% CO_2, 10% O_2 balanced in N_2,) and fast-SCR condition (▬: 200 ppm NO, 200 ppm NO_2, 400 ppm NH_3, 8% H_2O, 10% CO_2, 10% O_2 balanced in N_2).

outlet ratio of 0.6. In the same time, the C_2H_5OH conversion reached at 35%.

At t = 200 s, 400 ppm NH_3 was added to the reaction mixture ((EtOH + NH_3)-SCR, Table 1). Outlet profiles of NO and NO_2 dropped rapidly to quadrupled the NO_x conversion (up to 38%), together with NH_3 consumption. In parallel, ethanol and acetaldehyde outlet concentrations remained unchanged after few oscillations associated with gas feed stabilization. Obviously, NH_3 addition to EtOH-SCR system showed a dramatic benefit for the NO_x conversion at low temperature and in NO rich media.

This significant deNO_x enhancement is also reflected in a wider temperature range. Conversions of EtOH and NO_x for EtOH-SCR and (EtOH + NH_3)-SCR over Ag/Al catalyst are reported in Fig. 2. First, note that addition of NH_3 as co-reductant did not significantly affect the ethanol conversion profile (blue and red dotted lines). On the contrary, the NO_x conversion was remarkably enhanced, from 9% and 38% at 200 °C and 250 °C, respectively (blue full line), to 38% and 74% (red full line) when EtOH and NH_3 were co-fed. Above 350 °C, full NO_x conversion was achieved with or without NH_3 addition.

Interestingly, the NO_x conversion obtained with the (EtOH + NH_3)-SCR condition then fitted with the EtOH conversion, suggesting a beneficial effect of ethanol in the activation of ammonia to reduce NO_x over the Ag/Al_2O_3 material. This point is especially discussed Section 3.2 focussed on C-compounds distribution in EtOH-SCR and (EtOH + NH_3)-SCR conditions.

However, to put in evidence the collaborative effect of ethanol and NH_3 over Ag/Al, the NH_3-SCR behaviour was also examined on Ag/Al sample (experimental feed composition reported in Table 1). Results depicted in Fig. 3 indicate that when only NO was introduced as NO_x (orange line), the Ag/Al catalyst exhibited nearly no activity to reduce NO_x by NH_3. The NO_x conversion remained very low at 1–3% whatever the studied temperature. The ammonia conversion (not shown) followed the same trend, with a maximum NH_3 conversion of 4% at 500 °C. Note that the ammonia conversion was also close to zero without NO_x in the inlet mixture. These tests showed that this catalyst is unsuitable to activate neither the direct NO reduction by NH_3 nor the ammonia oxidation by O_2. Considering that EtOH-SCR led to high NO_2 formation which may be favourable to the NO_x reduction allowing the "fast-SCR" process, the Ag/Al catalyst was also evaluated in NH_3-SCR using a NO_2/NO_x inlet ratio of 0.5 (blue line, Fig. 3). Compared with the "standard NH_3-SCR" condition, the NO_x conversion by NH_3 was just a little improved and reached between 7% and 15% in the 200–500 °C temperature range. Again, the ammonia conversion remained close to that of NO_x, except for the higher temperatures. This poor activity of Ag/Al catalyst in NH_3-SCR is consistent with previously reported results [30–32] and demonstrates that the enhancement of the deNO_x efficiency in (EtOH + NH_3)-SCR conditions is not directly attributable to the NO_x reduction by NH_3.

3.2. Mechanistic study of the (EtOH + NH_3)-SCR process

3.2.1. C-compounds distribution in EtOH-SCR and (EtOH + NH_3)-SCR conditions

In order to obtain information about the reaction pathway involved in the (EtOH + NH_3)-SCR chemistry, the carbon compound distribution was examined depending on the presence of NH_3. Results are depicted in Fig. 4. As previously reported [10], ethanol was mainly converted into acetaldehyde at low temperature (T < 300 °C). Formaldehyde, ethylene were also detected, as well as traces of methanol (not shown).

In reaction mixture including NH_3 ((EtOH + NH_3)-SCR), no apparent alteration in both ethanol conversion and C-compounds selectivity was denoted. Consequently, there is no evidence for a reactivity between ammonia and organic species.

However, the possible formation of an organo-nitrogen intermediate species, obtained by reaction of ethanol with ammonia was supplementary checked by mass spectrometry analysis. In fact, ammonia condensation with aldehydes is well known to lead to imine compounds. The first step is a nucleophilic addition of

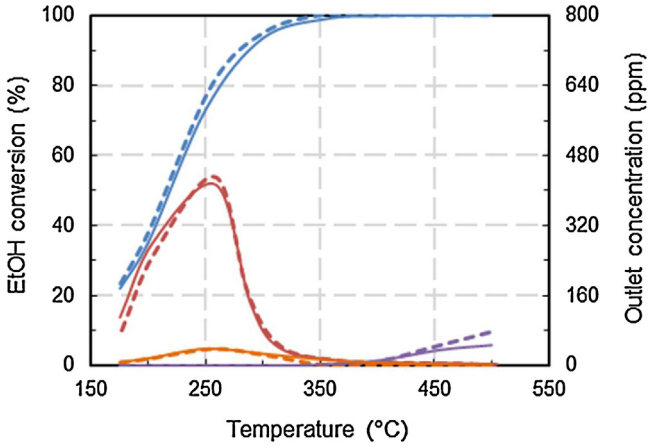

Fig. 4. Ethanol conversion (,) and C-compounds distribution (acetaldehyde (,); ethylene (,); formaldehyde (,)) over Ag/Al catalyst in EtOH-SCR (full lines) and (EtOH + NH_3)-SCR (dotted lines) conditions. (1200 ppm EtOH, with or without 400 ppm NH_3, 400 ppm NO, 8% H_2O, 10% CO_2, 10% O_2 balanced in N_2).

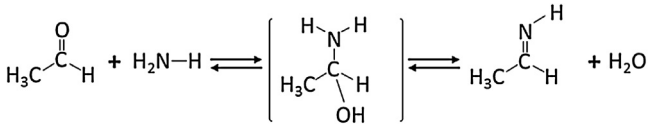

Scheme 1. Ethanimine formation mechanism.

primary amine like NH_3, to the carbonyl group of acetaldehyde, followed by a rapid proton transfer, as reported in Scheme 1 for ethanimine synthesis. In accordance with Vinogradoff *et al.* [42], the corresponding $m:z = 28$ value is expected as the main peak corresponding to the loss of CH_3 fragment from an alpha fragmentation of the ethanimine ($CH{=}NH^+$). The $m:z = 42$ and $m:z = 43$ value of $CH_3C{=}NH^+$ and $CH_3CH{=}NH^+$ respectively are also expected. Finally, none of these fragments were observed, giving no evidence of an organo-nitrogen compound formation and confirming that a direct reaction pathway between organic species and ammonia to enhance the NO_x reduction is invalidated.

3.2.2. NO_2 reactivity in (EtOH + NH_3)-SCR

As previously reported in Fig. 1, EtOH-SCR over Ag/Al sample revealed NO_2 emission of approximately 225 ppm at 200 °C. More precisely, the NO_2 emission reported in Fig. 5 depended on the temperature and varied together with the CH_3CHO profile (Fig. 4). As already reported in Ref. [10], the EtOH reaction pathway at low temperature (T < 300 °C) firstly involves a reaction between ethanol, NO and O_2 to produce acetaldehyde and NO_2 (Eq. (17)).

$$C_2H_5OH + NO + O_2 \rightarrow CH_3CHO + NO_2 + H_2O \quad (17)$$

Fig. 1 also showed that addition of NH_3 in the reaction mixture induced a decrease in NO_2 outlet concentration. Fig. 5 confirms that (EtOH + NH_3) co-injection (red curve, (EtOH + NH_3)-SCR) led to a significant decreases in NO_2 emission for all the studied temperature. This result suggests a reactivity between NH_3 and the *in situ* NO_2 formed from EtOH-SCR chemistry. Nevertheless, as previously discussed, the Ag/Al catalyst presented a poor activity in NH_3-SCR, even under the most favourable fast-SCR stoichiometry (Fig. 3), showing that NO_2 did not preferentially react with NH_3 over Ag/Al sample.

Subsequently, the influence of the inlet NH_3 concentration was studied in the low temperature range (175 °C–250 °C). The ammonia concentration was adjusted from 0 to 750 ppm in addition to the gas mixture corresponding to EtOH-SCR condition (Table 1).

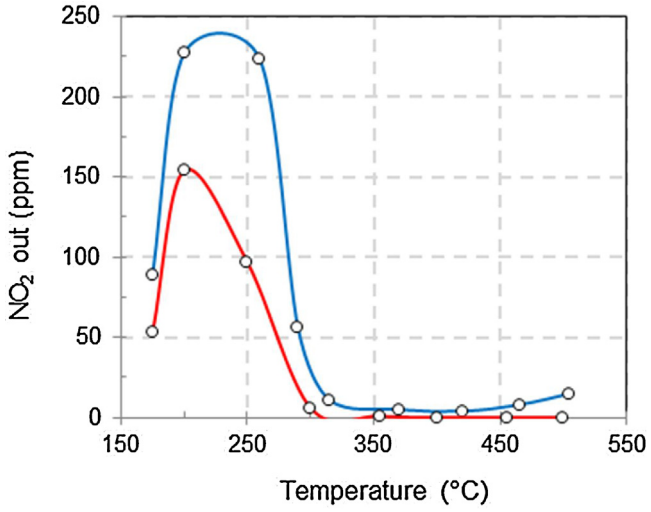

Fig. 5. NO_2 outlet emission over Ag/Al catalyst: Reaction mixture: ( ) EtOH-SCR (400 ppm NO, 1200 ppm C_2H_5OH, 8% H_2O, 10% CO_2, 10% O_2 balanced in N_2); ( ) (EtOH + NH_3)-SCR (400 ppm NO, 1200 ppm C_2H_5OH, 400 ppm NH_3, 8% H_2O, 10% CO_2, 10% O_2 balanced in N_2).

Results are presented in Fig. 6. As expected, the NO_x conversion increased with temperature, and it clearly appears that the gain in NO_x conversion in regard on the amount of added ammonia is strongly temperature dependant, even in a rather small temperature range (175–250 °C). Interestingly, Fig. 6 clearly shows that NO_2 is the main compound affected by the NH_3 addition, especially with the increase of the temperature. It indicates that ammonia reacted preferentially with NO_2 in ethanol media, even if the Fast-NH_3-SCR test previously depicted in Fig. 3 showed a limited activity. In line with this observation, the calculated ratio between the amount of converted ammonia and the amount of supplementary converted NO_x also increased with the temperature. It was close to 1 at 175 °C (with a quite large uncertainty because ammonia and NO_x variations were then limited), increased to 1.1–1.2 at 200 °C and reached 1.3–1.4 at 250 °C, without clear evidence of the ammonia inlet concentration. Then, the apparent NH_3—NO_x stoichiometry appeared to vary from a fast/standard-SCR stoichiometry at 200 °C to an additional contribution of a NH_3—NO_2 reaction with the increase of temperature.

Lastly, whatever the temperature between 175 °C and 250 °C, the ethanol outlet concentration (not shown) appears unaffected by the amount of added ammonia.

To further study the interactions between ammonia, ethanol and NO_x on Ag/Al catalyst, adsorption of these molecules was monitored by Infrared Spectroscopy.

3.2.3. Infrared spectroscopy study

3.2.3.1. NH_3 adsorption. NH_3 adsorption over Ag/Al sample was firstly studied. Spectra (not shown) are remarkable by low intensive bands due to the weak acidity of alumina to adsorb ammonia at 200 °C. Nevertheless, ammonia is apparently adsorbed on both Lewis and Brønsted acid sites. The bands at 1228 and 1288 cm^{-1} are attributed to the symmetric deformation of NH_3 ($\delta_s(NH_3)$) coordinatively bound to Lewis acid sites on Ag/Al_2O_3. Note that the symmetric deformation vibration is the more sensitive mode to the strength of the Lewis acid-base interaction. The two components observed at 1228 and 1288 cm^{-1} probably reveal ammonia coordination onto tetrahedral Al^{3+} and octahedral Al^{3+} Lewis acid sites of different strength. The band at 1579 cm^{-1} is due to the asymmetric deformation of NH_3 ($\delta_{as}(NH_3)$) adsorbed on Lewis acid sites on the catalyst surface. Two bands at 1684 and 1628 cm^{-1} are attributed to $\delta_s(NH_4^+)$

Table 2
Infrared bands attribution for adsorbed species and free OH groups on Ag/Al_2O_3.

Gas mixture	Surface species		Assignment	Wavenumber (cm^{-1})
	Type Ib $(Al_{VI})OH$		$\nu_{(OH)}$	3800–3785
	Type Ia $(Al_{IV})OH$		$\nu_{(OH)}$	3780–3760
	Type IIb $(Al_{VI})_2OH$		$\nu_{(OH)}$	3745–3740
	Type IIa $(Al_{IV}Al_{VI})OH$		$\nu_{(OH)}$	3735–3720
	Type III $(Al_{VI})_3OH$		$\nu_{(OH)}$	3710–3680
$(EtOH—O_2)$	Enolic	$(CH_2—CH—O)^-$	$\nu_{as(CCO)}$	1629
	Acetate	$(CH_3\text{-}(C=O)\text{-}O)^-$	$\nu_{as(OCO)}$	1588
	Acetate	$(CH_3\text{-}(C=O)\text{-}O)^-$	$\nu_{s(OCO)}$	1463
	Enolic	$(CH_2—CH—O)^-$	$\nu_{s(CCO)}$	1391
	Enolic	$(CH_2—CH—O)^-$	$\delta_{(CH)}$	1333
$(NO—O_2)$	Monodentate		$\nu_{3'}$	1547–1562
	Nitrate		$\nu_{3''}$	1299–1289
	Bidentate		$\nu_{3'}$	1587–1583
	Nitrate		$\nu_{3''}$	1254–1244
	Bridged Nitrate		$\nu_{3'}$	1612
	Monodentate		ν_1	1313
	Nitrite		ν_3	1229
(NH_3)	Ammonium ion (Brønsted AS)		$\delta_{s(NH4^+)}$	1684
	Coordinated ammonia (Lewis AS)		$\delta_{as(NH3)}$	1628
	Coordinated ammonia (Lewis AS)		$\delta_{as(NH3)}$	1579
	Ammonium ion (Brønsted AS)		$\delta_{as(NH4^+)}$	1395
	Coordinated ammonia (Lewis AS)		$\delta_{s(NH3)}$	1288
	Coordinated ammonia (Lewis AS)		$\delta_{s(NH3)}$	1228

and $\delta_{as}(NH_4^+)$ bound onto Brønsted acid sites respectively. The peak at 1395 cm^{-1} is assigned to NH_4^+ species on Al_2O_3 support ($\delta_{as}(NH_4^+)$ [43,44–46]. The corresponding assignments are reported Table 2.

3.2.3.2. EtOH-O_2 co-adsorption. IR spectra of $(EtOH\text{-}O_2)$ adsorption at equilibrium (Fig. 7A black full line) results in the appearance of several bands at 1629, 1588, 1463, 1391 and 1333 cm^{-1}. Assignments are reported in Table 2. In accordance with results reported in previous study for acetic acid adsorption, the bands at 1588 and 1463 cm^{-1} are assigned to adsorbed acetate ($\nu_{as(OCO)}$ and $\nu_{s(OCO)}$ respectively) [47]. In addition, bands at 1629, 1391 and 1333 cm^{-1} are clearly observed. The band at 1629 cm^{-1} is assigned to asymmetric stretching vibration mode ($\nu_{as(CCO)}$) and peaks at 1391 and 1333 cm^{-1} is attributed to a symmetric stretching vibration ($\nu_{s(CCO)}$) mode and to a C—H deformation mode ($\delta_{(CH)}$) of enolic species $(CH_2—CH—O)^-$, respectively. Several bands are observed around 1800–1700 cm^{-1} and 1300–1200 cm^{-1} which are assigned to acetaldehyde gas species. These bands disappear after evacuation.

3.2.3.3. NH_3 adsorption over (EtOH-O_2) ad-species. As shown in Fig. 7A, the adsorption of ammonia (10 hPa at equilibrium) on ethanol-covered Ag/Al_2O_3 surface leads to decrease the intensity of the bands at 1629, 1391 and 1333 cm^{-1} previously attributed to enolic species. It means that, without NO_x compounds, ammonia reacts preferentially with ethoxy species than with acetate. This is highlighted by subtracting spectra obtained after adsorption of ethanol and ammonia (shown in bold gray line). The negative absorption bands show the consumption of the enolic species by ammonia. Note that the IR vibration mode of ammonia is not observed.

3.2.3.4. (NO-O_2) adsorption. It is well-known that NO_2 and NO can react on metal oxide surfaces to yield a number of different surface species that in principle can be differentiated by infrared spectroscopy and results in different absorption frequencies in the spectral range from 1200 to 1700 cm^{-1}. Nitrogen dioxide adsorption can result in the formation of both adsorbed nitrate (NO_3^-) and nitrite (NO_2^-). The coordination of nitrate, nitrite, and nitric oxide in inorganic complexes has been discussed in the literature in detail and provides a useful guide for the interpretation of the infrared absorption bands of adsorbed species [48–50]. It is reported that the planar nitrate ion belongs to the point group D_{3h} and has four fundamental vibrations: ν_1 (symmetric stretch), ν_2 (out-of-plane bend), ν_3 (asymmetric stretch), and ν_4 (in-plane bend). The last three are infrared active. The surface interaction with NO_2 or $(NO + O_2)$ leads to the reduction of the nitrate ion symmetry from D_{3h} to C_{2v} and causes the degenerated ν_3 mode to split into four modes, of which two are IR active (ν_3' and ν_3'' for the high and low-frequency component respectively).

IR spectra of adsorbed N-containing species after an exposure of Ag/Al_2O_3 to $(NO—O_2)$ are reported in Fig. 7B (black dotted line). After the first adsorption dose (spectra not shown), spectrum is remarkable by bands at 1313 and 1229 cm^{-1}. The band observed at 1229 cm^{-1} is assigned to the asymmetric stretch vibration (ν_3)

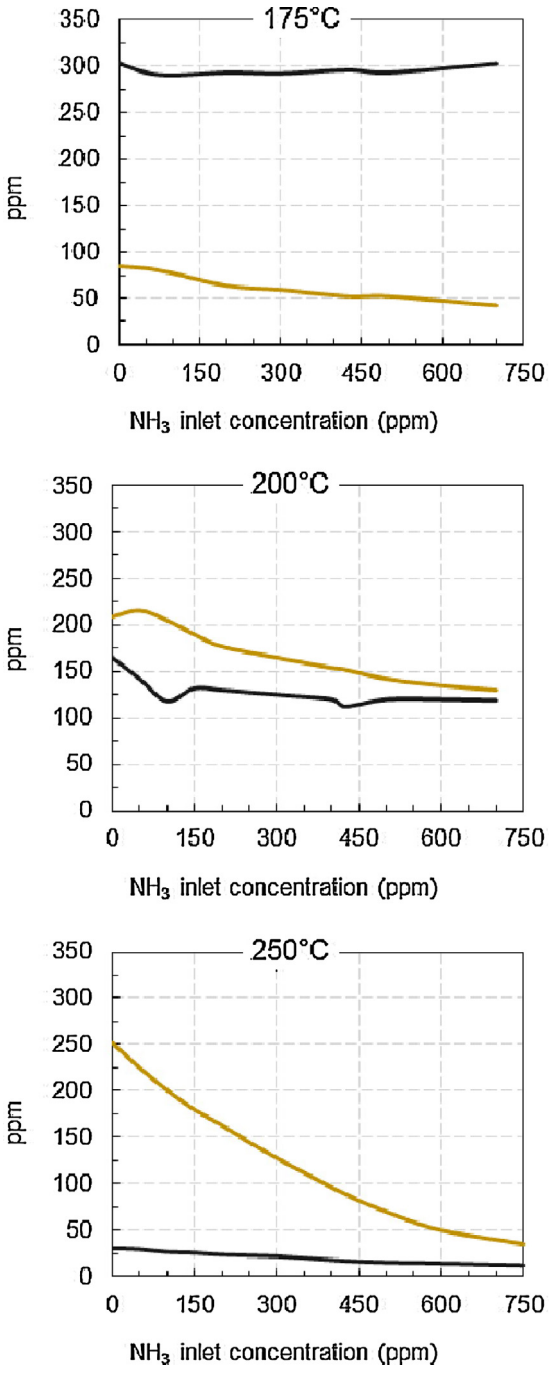

Fig. 6. Effect of NH_3 inlet concentration in NO (▬) and NO_2 (▬) outlet emissions at 175, 200 and 250 °C for (EtOH + NH_3)-SCR process over Ag/Al catalyst.

of the nitrite ion; the band at 1313 cm^{-1} to the symmetric stretching vibration (ν_1). For higher (NO—O_2) coverage, several absorption bands are observed, unanimous assigned to nitrates species by many authors despite some inconsistencies. For instance, Venkov et al. [45] assigned the band at 1627 (ν_3') and 1261 cm^{-1} (ν_3'') to bridged nitrates while the bands at 1593 (ν_3') and 1296 cm^{-1} (ν_3'') are due to bidentate nitrate. The bands at 1562 cm^{-1} associated with one component around 1300 cm^{-1} corresponds to monodentate nitrate. Note that a similar coincidence between the ν_3'' vibrations of mono- and bidentate nitrates was reported in this work. Yu et al. [51] observed monodentate (1560, 1250 cm^{-1}), bidentate (1583, 1302 cm^{-1}), and bridging (1612 cm^{-1}) nitrates after an exposure of the Ag/Al_2O_3 to NO + O_2. Tamm et al. [52] assigned the high-frequency component (ν_3') at 1611, 1586 and

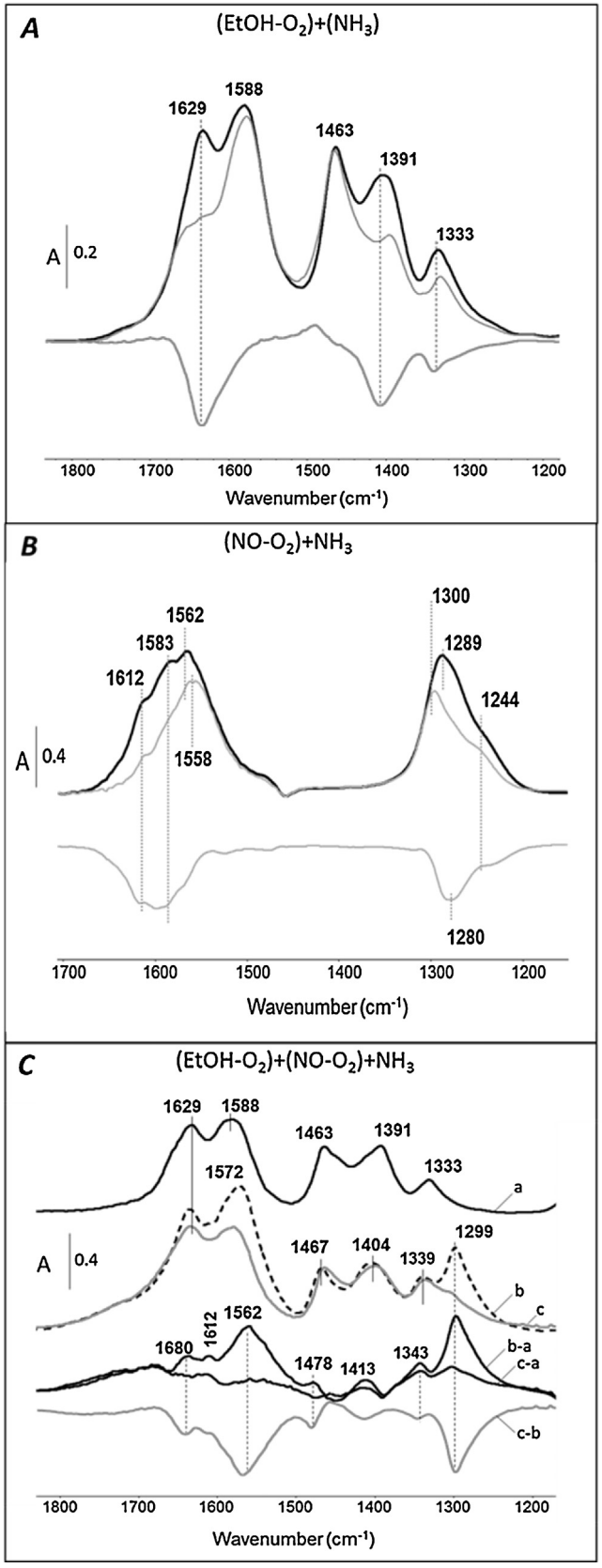

Fig. 7. Transmission IR spectra of co-reactive compounds adsorption at 200 °C over Ag/Al catalyst. (A): (EtOH-O_2) + (NH_3); (B): (NO-O_2) + (NH_3); (C): (EtOH-O_2) + (NO-O_2) + (NH_3). (10 hPa at equilibrium).

1546 cm^{-1} to bridge-bound, bidentate and monodentate nitrates species respectively associated to the low-frequency component at 1250 cm^{-1} (bidentate) and 1304 cm^{-1} (monodentate)

Finally, in this work, the assignments reported in Table 2 are proposed. The bands at 1254 and 1587 cm^{-1} and the bands at 1299 and 1547 cm^{-1} growth simultaneously, which indicates that they either correspond to two surface species. With ($NO + O_2$) coverage increase, these bands are shifted to 1244/1583 cm^{-1} and 1289/1562 cm^{-1} (black full line). In agreement with data from the literature, the bands with maxima at 1562 and 1289 cm^{-1} are attributed to monodentate nitrate, and the doublet at 1583 and 1244 cm^{-1} to bidentate nitrates. The bands at 1612 cm^{-1} is assigned to bridging nitrates.

3.2.3.5. NH_3 adsorption over (NO-O_2) ad-species. After adsorption of (NO-O_2) at equilibrium (10 hPa, bold black line, Fig. 7B), the co-adsorption of ammonia (10 hPa, gray line) was performed. It induced a decrease of the intensity of the high-frequency component (ν_3') of bridged (1612 cm^{-1}) and bidentate (1583 cm^{-1}) nitrates, but without a full consumption of adsorbed NO_x compounds after two hours at 200 °C. The ν_3'' band at 1289 cm^{-1} is shifted to higher frequency of about 1300 cm^{-1}. Note that the $\delta_{s(NH3)}$ vibration mode of coordinated ammonia can be superimposed to the degenerated ν_3'' mode of adsorbed monodentate nitrate.

More precisely, the negative bands near 1612, 1583 and 1280 cm^{-1} illustrates that bridged and bidentate nitrates are preferentially consumed by ammonia co-adsorption. The higher stability of the monodentate nitrate is in accordance with previous literature data [49]. This result shows a direct interaction between nitrates (preferentially bidentate and bridged) and NH_3 on the catalyst surface.

3.2.3.6. Effect of NH_3 adsorption over ($EtOH$-O_2)+(NO-O_2) ad-species. Resulting IR spectra for ($EtOH$-O_2)+(NO-O_2)+NH_3 are presented in Fig. 7C. The black full line (spectrum a) corresponds to the spectrum recorded after $EtOH$-O_2 adsorption that is consistent with results already discussed in Fig. 9A. After evacuation and co-adsorption of NO-O_2, the spectrum in black dotted line (b) exhibited a new band at 1299 cm^{-1}which is attributed to ν_3'' of monodentate nitrate. The corresponding ν_3' overlaps in the $\nu_{as(OCO)}$ of adsorbed acetate species (1588 cm^{-1}). To highlight adsorbed species resulting of the co-adsorption of ($EtOH$-O_2) and (NO-O_2), these two spectra were subtracted (b-a). Nitrates species are then clearly distinguished by bands at 1612 cm^{-1} ($\nu_{3'}$ bridged nitrates) and 1562 cm^{-1} ($\nu_{3'}$ monodentate nitrates). Co-adsorption of NH_3 (spectra c, c-a and c-b), results in a strong decrease of all the bands assigned to the nitrate species. Unlike co-adsorption (NO-O_2)+(NH_3), the presence of enolic and acetates species on the catalyst surface greatly enhanced the reduction of nitrates with ammonia. In addition, the affected species are different, monodentate nitrates were almost fully consumed by NH_3 in presence of EtOH.

3.2.3.7. OH and NH stretching modes. . In Fig. 8 is presented IR spectra recorded in the 3900–3000 cm^{-1} spectral range ($\nu_{(OH)}$ and $\nu_{(NH)}$) for the following gas mixture co-adsorption: NO-O_2, NO-O_2 + NH_3, $EtOH$-O_2 + NH_3 and $EtOH$-O_2 + NO-O_2 + NH_3. IR spectra are remarkable by NH stretching bands at 3390 and 3290 cm^{-1} assigned to coordinated ammonia. These bands are not observed when ammonia is adsorbed alone (without NO_x pre-adsorption; spectra not shown). Thus, it is proposed that when nitrates are formed, due to their negative induction effect, they withdraw electron density from nearby Al^{3+} cation. As a result, the Lewis acidity of the latter increases and nitrosyl complexes/ammonia adsorption is probably formed.

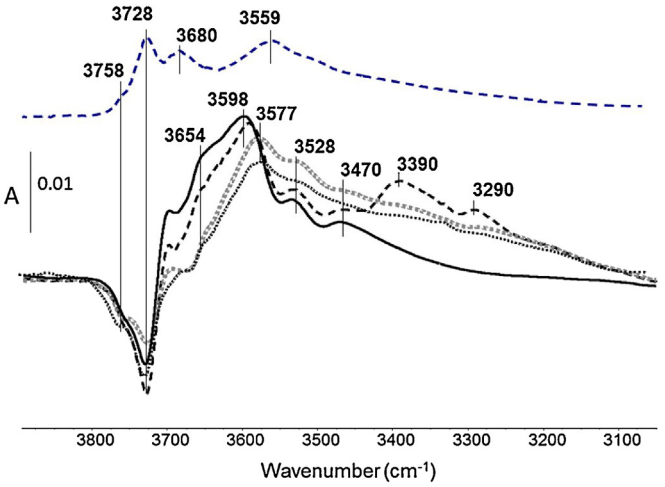

Fig. 8. IR spectra at 200 °C in $\nu_{(OH)}$ and $\nu_{(NH)}$ stretching region over Ag/Al catalyst. ▬ : reference spectrum after calcination (400 °C under vacuum); ▬ : (NO-O_2) adsorbed species; ▬ : (NO-O_2)+(NH_3) adsorbed species; ▬ : ($EtOH$-O_2)+(NH_3) adsorbed species ▬ : ($EtOH$-O_2)+(NO-O_2)+(NH_3) adsorbed species.

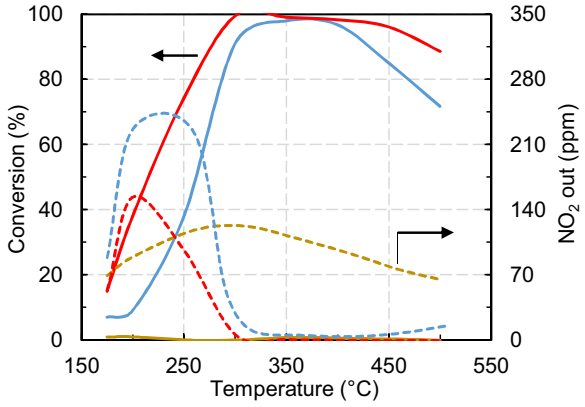

Fig. 9. NO_x conversion (full line) and NO_2 emission (dotted line) over Ag/Al catalyst for H_2-SCR (▬), EtOH-SCR (▬) and EtOH + NH_3-SCR (▬).

Additionally, OH groups of alumina are characterized by complex O—H stretching band in the 3900–3500 cm^{-1} zone. The assignment of these bands was largely studied in the literature but is still controversial. Among the various proposed models, the most used was proposed by Tsyganenko et al. [53,54] and completed by Knözinger et al. [55]. Five types of OH species were identified on the surface of alumina layers, depending firstly on the number of Al^{3+} bonding to the OH group and secondly on the coordination number of the Al^{3+} ion. This model was used in this work to study the free OH group of silver supported alumina catalyst. IR spectra reported Fig. 8 are consistent with those reported in the literature, showing the different types of OH groups of alumina that display bands at 3758, 3728 and 3680 cm^{-1}. Assignments are reported in Table 2.

In addition, Fig. 8 indicates that adsorption of reactive species (NO-O_2, $EtOH$-O_2) led to the decrease of peaks at 3758 cm^{-1} and 3728 cm^{-1} attributed to a loss of OH surface species. These absorption bands have been described before [56] and correspond to the O—H stretching vibration of OH groups coordinated with one aluminum atom in coordination states IV (Type Ia), and with two aluminum atoms in coordination IV and VI (type IIa), respectively.

Interestingly, new OH bands at 3598-3577, 3528, and 3470 cm^{-1} are observed. These bands can be assigned to the O—H vibration of hydrogen-bonded OH groups of acids, such as HNO_3 or HONO [47]. The observed acidic OH vibrations (3600–3400 cm^{-1}) are caused by adsorbed HNO_3 or HONO, which are in equilibrium with nitrate

and nitrite ions and surface-adsorbed water observed at 3559 cm^{-1}. These new intermediate species are especially observed after EtOH adsorption (gray dotted line). It suggests that resulting ethanol ad-species enhance the reactivity of NO_x compounds.

To conclude, IR characterization reveals that ammonia is highly reactive towards enolic ad-species. In addition, bridged and bidentate nitrates are preferentially consumed by ammonia co-adsorption, but are still observed in absence of ethanol. Finally, over surface pre-exposed to ethanol, the reactivity of NH_3 with nitrates compounds is enhanced and intermediates HONO or HNO_3, commonly reported as intermediates in NO_x SCR pathway, are observed.

3.2.4. Role of H^* intermediate species

IR characterization showed that ethanol ad-species are involved in the reduction of NO_x compounds by NH_3 in the (EtOH + NH_3)-SCR process. As mentioned in the introduction part, the first step of the EtOH-SCR framework results in C_2H_5OH dissociative adsorption into surface ethoxide $C_2H_5O^*$ and surface hydrogen H^* species (Eq. (11)) [10,24,26,57]. Thereafter, ethoxide is converted into acetaldehyde (Eq. (12)) providing a second surface-bound hydrogen ad-atoms. Fig. 4 shows that acetaldehyde emission started from 175 °C (lowest tested temperature) and reached a maximum at 250 °C, indicating that hydrogen ad-atoms should be available at low temperature. Addition of hydrogen into the reaction mixture was reported to enhance the deNO_x efficiency in EtOH-SCR process. It was advanced that H_2 addition promotes the partial oxidation of C_2H_5OH to form enolic species which mainly contribute to accelerate NO_x reduction [29,58,59]. Additionally, Flura et al. [10] observed that NO oxidation into NO_2 was enhanced in presence of small amounts of H_2 (167 ppm) over silver supported catalyst. It was proposed that hydrogen is able to reduce silver particles, leading to higher oxidation performances. It is also likely that hydrogen favours the nitrates species desorption. The promotion effect of H_2 co-feeding was also evidenced in hydrocarbon-SCR, with an enhancement of the deNO_x activity at low temperature [60]. However, the most significant impact of H_2 addition is observed on the H_2-assisted NH_3-SCR process over Ag/Al_2O_3 catalysts [24,32,61,62]. Consequently, the H_2 behaviour in NO reduction was examined and compared to the previously studied reductant mixture.

First, the deNO_x efficiency of Ag/Al catalyst was evaluated in H_2-SCR. Fig. 9 reports the NO_x conversion (full line) and the NO_2 emission (dotted line) for H_2-SCR, EtOH-SCR and EtOH + NH_3-SCR. As expected, no deNO_x activity was observed in H_2-SCR condition (brown curve). Formation of NO_2 was observed, but in a lower extent than in EtOH-SCR condition, with maximum concentrations of 130 ppm for H_2-SCR (at 300 °C, brown dotted line), compared with 250 ppm for EtOH-SCR (at 200 °C blue dotted line). These results support the high reactivity of ethanol to oxide NO and provide NO_2 at low temperature (Eq. (17)). More interestingly, these experiments demonstrates that the hydrogen H^* species provided by the ethanol dehydrogenation do not directly act as NO_x reductant over Ag/Al but would rather be involved during the (EtOH + NH_3)-SCR process (red curve).

To highlight the reactivity of hydrogen in the NO_x reduction process by NH_3, the reactivity of Ag/Al sample was investigated in H_2-assisted NH_3-SCR and compared with both EtOH-SCR and (EtOH + NH_3)-SCR (Table 3). The H_2 concentration was fixed in regard on the activity of ethanol dehydrogenation, *i.e.* at 100 ppm and 270 ppm for temperature test of 175 °C and 200 °C, respectively. Compared with EtOH-SCR, NH_3 addition induced an enhancement of the NO_x conversion of 8% and 25% at 175 °C and 200 °C, respectively. Interestingly, similar deNO_x improvement was obtained in H_2-assisted NH_3-SCR despite the low H_2 concentration used. It clearly indicates that the deNO_x enhancement supplied by the NH_3 addition to EtOH-SCR is related to the H^* species formed during ethanol oxidation.

3.2.5. Proposed reaction pathways

The enhancement of NO_x conversion by NH_3 co-feeding in EtOH-SCR over Ag/Al catalyst is clearly evidenced (Fig. 2). However, no reactivity of ammonia with carbon-based by-products was observed. It means that NH_3 did not react to produce organo-nitrogen reactive intermediate. In addition, Ag/Al sample was not significantly active to reduce NO_x by NH_3. Obviously, NH_3 is activated over Ag/Al catalysts only in the presence of ethanol. Moreover, the highly beneficial effect of H_2 addition on the NH_3-SCR process over Ag/Al_2O_3 catalysts is well documented and the observed improvement in (EtOH + NH_3)-SCR over Ag/Al is consistent with the amount of H^* species obtained from ethanol dehydrogenation into acetaldehyde (see Section 3.2.4). Besides, IR results evidence the formation of HONO/HNO_3 intermediates when ethanol and NO are co-adsorbed.

Consequently, taking into account all the data presented in this work, it is proposed that the hydrogen H^* species provided by the ethanol dehydrogenation are the main responsible for the high deNO_x efficiency at low temperature observed in the (EtOH + NH_3)-SCR experiments. Based on the mechanism presented in the introduction part, it is assumed that the HONO/HNO_3 route formation is a determining step to the NO_x reduction by NH_3. The effect of H^* species are tentatively attributed to an activation of the NO oxidation into reactive intermediate N-containing species, such as HONO and/or HNO_3, evidenced by FTIR experiments (Fig. 7). Ammonium nitrite formation (Eq. (6)), which is described as the penultimate step of deNO_x chemistry with many practical catalysts, can subsequently be formed by reaction of NH_3 with nitrous acid [63].

Finally, the proposed (EtOH + NH_3)-SCR process avoids the rate-limiting step of nitromethane formation by three different routes (Scheme 2). The N_2 route formation originated from EtOH-SCR (blue route in Scheme 2) is limited at low temperature by the CH_3NO_2 rate-determining step. Ammonia formation is obtained only for T > 250 °C [23]. Gaseous NH_3 addition helps to avoid this problem. Actually, the deNO_x efficiency improvement in the (EtOH + NH_3)-SCR process is not determined by the efficiency of Ag/Al sample to directly reduce NO_x by NH_3. In fact, the NH_3-SCR route (green dotted route in Scheme 2), only active when NO_2 is formed during EtOH-SCR, has only few influence on the overall efficiency of the system. Finally, the remarkable NO_x conversion achieved with the NH_3 co-feeding is assigned to the formation of HNO_x species, obtained by the generation of H^* compound from the dehydrogenation of ethanol. Ethanol can therefore be seen as a hydrogen provider, in addition to induce the oxidation of NO into NO_2. The added ammonia can then follow the conventional mechanism of H_2-assisted NH_3-SCR exposed in the literature. This system allows the *in situ* generation at low temperature of the key intermediates of the deNO_x chemistry over Ag/Al sample (red route in Scheme 2).

With a conversion ranging from 15 to 75% in the 175–250 °C region, this system is efficient for NO_x removal using only NO as NO_x. However, this system can be further optimized by means of a dual-bed configuration, exposed in the next section.

3.3. DeNO_x efficiency improvement of the (EtOH + NH_3)-SCR process: dual-bed configuration

In this section, the (EtOH + NH_3)-SCR process is extended to a more complex catalytic system to obtain a supplementary enhancement of the NO_x conversion at low temperature (175–300 °C) using the same ethanol-NH_3 mixture. In fact, in (EtOH + NH_3)-SCR process over Ag/Al, the outlet exhaust gas still contained some NH_3 and NO_x

Table 3
NO_x conversions at 175 and 200 °C in EtOH-SCR (1200 ppm C_2H_5OH), in NH_3-assisted EtOH-SCR (1200 ppm C_2H_5OH + 400 ppm NH_3) and in H_2-assisted NH_3-SCR (400 ppm NH_3 + 100–270 ppm H_2) processes blended in 400 ppm NO, 8% H_2O, 10% CO_2, 10% O_2.

Temperature (°C)	NO_x conv. EtOH-SCR (%)	NO_x conv. EtOH/NH_3-SCR (%)	NO_x conv. gain by NH_3 add. in EtOH-SCR[a] (%)	NO_x conv. H_2-assisted NH_3-SCR[b] (%)
175	7	15	8	9
200	9	38	29	27

[a] Difference between NO_x conv. in EtOH-SCR with or without NH_3 addition.
[b] H_2 amount corresponds to the quantity potentially produced by EtOH oxidation to CH_3CHO during EtOH-SCR process (100 ppm H_2 at 175 °C; 270 ppm H_2 at 200 °C).

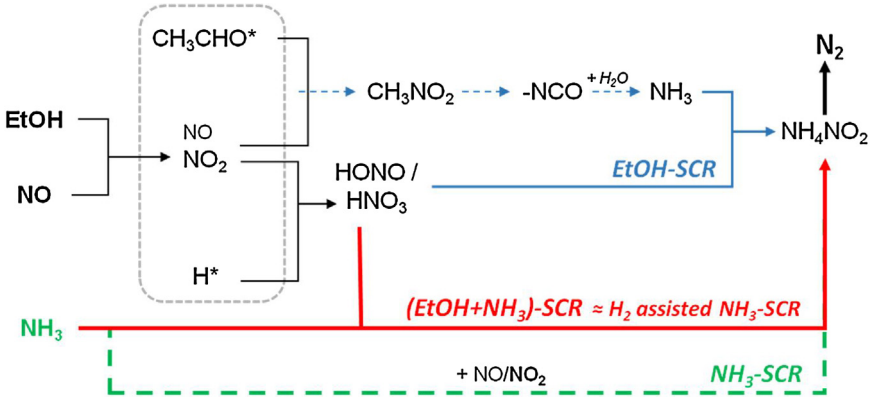

Scheme 2. Proposal of reaction pathway in EtOH + NH_3-SCR over Ag/Al catalyst.

(especially including NO_2) in this low temperature range. Consequently, a dedicated SCR catalyst placed downstream the Ag/Al_2O_3 catalyst was supposed to allow both a supplementary NO_x abatement together with an ammonia slip restraint. Supported transition metal, ceria based oxides such as $Fe_2O_3/WO_3/ZrO_2$ [38], MnO_x-CeO_2 [39] or $WO_3/Ce_xZr_{1-x}O_2$ [40] or metal exchanged zeolite [20] are active materials for this purpose. $WO_3/Ce_xZr_{1-x}O_2$ catalyst was selected in this work as NH_3-SCR material, since it appeared to be active with various NO_2/NO_x inlet ratio including the standard-SCR stoichiometry. Moreover, this catalyst may also act as an ammonia slip catalyst since it was reported to be active in NH_3 oxidation by O_2, with a full selectivity into N_2 [40].

First, single WO_3/Ce-Zr catalyst was evaluated in EtOH-SCR and (EtOH + NH_3)-SCR with only NO as injected NO_x (SI file, Fig. S3). The NO_x conversion obtained with only ethanol as reductant was very limited, with a maximum of only 7% recorded at 300 °C. This WO_3/Ce-Zr catalyst is then poorly active in NO_x reduction by ethanol. To the opposite, the NO_x conversion was significant in (EtOH + NH_3)-SCR condition, from 13 to 70% in the 175–450 °C temperature range. Interestingly, this catalyst is very active in Fast-NH_3-SCR condition, with NO_x conversion of 53% and 90% at 170 °C and 200 °C, respectively.

Fig. 10 reports the NO_x conversion obtained in (EtOH + NH_3)-SCR over the Ag/Al + WO_3/Ce-Zr dual bed system. Compared with Ag/Al alone, a remarkable supplementary NO_x conversion was obtained at low temperature. The NO_x conversion was then ranked between 46 and 95% in the 175–250 °C temperature range, while only NO was initially injected. As expected, supplementary ammonia consumption was also observed in the dual bed system. At 200 °C, the overall NH_3-NO_x stoichiometry respected a ratio close to 1–1. Consequently, the low temperature ammonia slip was limited, at only 115 ppm and 125 ppm NH_3 at 200 °C and 250 °C, respectively (Fig. 10). For Temperature higher than 350 °C, the ammonia over injection was factually not needed since the NO_x conversion already reached 100% with ethanol. Moreover, *in situ* produced ammonia is emitted from Ag/Al (Fig. 10)., as previously reported [23]. For instance, at 350 °C, the WO_3/Ce-Zr catalyst is virtually submitted to 400 ppm NH_3 from ammonia co-injection plus 150 ppm NH_3 from

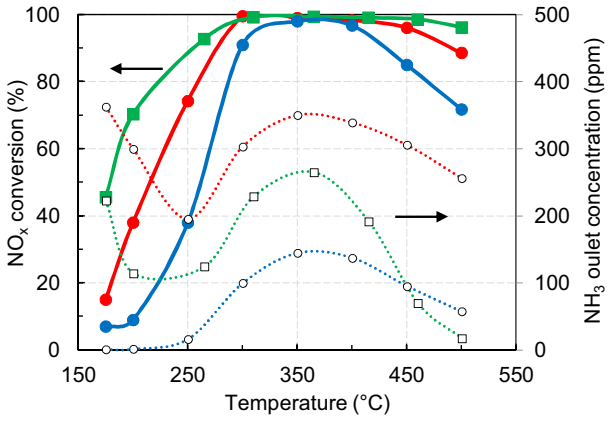

Fig. 10. NO_x conversion (full line) and NH_3 oulet concentration (dotted line) in EtOH-SCR (▬) and (EtOH + NH_3)-SCR (▬) over Ag/Al sample (○), and in (EtOH + NH_3)-SCR condition over Ag/Al + WO_3/Ce-Zr (□) dual bed system (▬).

the EtOH process over Ag/Al. However, WO_3/Ce-Zr then acted as an ammonia slip catalyst since approximately 50% of this 550 ppm ammonia excess appeared converted into N_2. This apparent conversion rate reached 86% at 450 °C Nevertheless, taking into account the whole temperature range, the (EtOH + NH_3)/NO_x ratio should to be adjusted (*i.e.* decreased) depending on the temperature to prevent ammonia emission.

Besides, over the Ag/Al + WO_3/Ce-Zr dual bed system, NO_2 emitted from the first catalytic bed (Ag/Al sample, Fig. 5, red line) was fully converted over the downstream WO_3/Ce-Zr material (SI file Fig. S4). Nevertheless, the NH_3-NO-NO_2 stoichiometry over the WO_3/Ce-Zr sample did not correspond to only the fast SCR reaction, NO_2 appeared partially reduced into NO: at 200 °C, 128 ppm NO_x are supplementary converted into N_2 in the dual-bed configuration, while 154 ppm NO_2 and 285 ppm NH_3 are converted.

In order to confirm that the efficiency gain observed in Fig. 10 arose from a synergy effect between the two catalytic materials Ag/Al and WO_3/Ce-Zr, (EtOH + NH_3)-SCR experiments were performed over single Ag/Al and WO_3/Ce-Zr catalysts with doubled

catalytic weight (200 mg), *i.e.* with the same catalyst weight/molar flow (W/F) ratio than for the dual bed set-up. Results presented in SI file (Fig. S5) indicate significantly lower deNO$_x$ efficiency in the 175–250 °C temperature range over single catalysts compared with the dual-bed system. Obviously, this result illustrates the benefit of the (EtOH + NH$_3$)-SCR process with the dual bed configuration.

Finally, the deNO$_x$ efficiency obtained in (EtOH + NH$_3$)-SCR condition over the dual-bed system was similar to the activity observed in the most favourable fast-SCR stoichiometry over single WO$_3$/Ce-Zr sample reported in SI file, Fig. S3. This result is also better than that obtained over a patented iron exchanged ferrierite (Fe/FER) using the same set-up. In fact, results reported in [64] and in Fig. S6 show that the NO$_x$ conversion in standard-SCR condition is limited from 58 to 69% in the 200–500 °C temperature range. A 2.8%Cu/FER was also evaluated and exhibited conversions close to Ag/Al in (EtOH + NH$_3$)-SCR condition (Fig. S6), without reaching the efficiency reported on the combined Ag/Al + WO$_3$/Ce-Zr in (EtOH + NH$_3$)-SCR condition.

To conclude, a remarkable deNO$_x$ efficiency was obtained at low temperature over Ag/Al + WO$_3$/Ce-Zr dual bed catalysts devoted to the (EtOH + NH$_3$)-SCR process. NO$_x$ conversion then reached 70% at 200 °C, compared with 7% in EtOH-SCR over Ag/Al. Additionally, the deNO$_x$ efficiency of this (EtOH + NH$_3$)-SCR process is no longer determined by the activity of the upstream oxidation catalyst (DOC) since results presented in this work were without NO$_2$ in the inlet feed stream.

4. Conclusion

This work demonstrates that co-feeding ammonia and ethanol on a Ag/Al$_2$O$_3$ catalyst enables a drastic enhancement of the NO$_x$ conversion at low temperature (175–250 °C) using only NO as NO$_x$ (standard SCR condition). The (EtOH + NH$_3$)-SCR over Ag/Al catalyst has superior NO$_x$ reduction efficiency than both NH$_3$-SCR and EtOH-SCR in the temperature range 175–500 °C. It is proposed that the hydrogen H* species provided at low temperature by the ethanol dehydrogenation is the main responsible for the deNO$_x$ efficiency improvement, in addition to the beneficial concomitant NO$_2$ formation observed at low temperature with ethanol. Further deNO$_x$ improvement was obtained over a dual-coupled catalytic system composed of Ag/Al and a usual NH$_3$-SCR catalyst (WO$_3$/Ce-Zr), taking advantage of the remaining NH$_3$ and NO$_2$ from Ag/Al catalyst. A promising efficiency of 70% of NO$_x$ converted at 200 °C was reached, without dependence to the activity of the upstream oxidation catalyst (DOC).

The present results also have practical implications. A unique aqueous solution containing both urea (NH$_3$ carrier) and ethanol could be used for this purpose, also allowing carrying away a much higher amount of reductant species versus the conventional AdBlue solution.

Acknowledgment

Authors thank the Regional Council of Poitou-Charentes and the French Ministry of Researchfor financial support.

Appendix A. Supplementary data

Supplementary data associated with this article can be found, in the online version, at http://dx.doi.org/10.1016/j.apcatb.2017.08.015.

References

[1] R.N. Colvile, E.J. Hutchinson, J.S. Mindell, R.F. Warren, Atmos. Environ. 35 (2001) 1537–1565.
[2] G.M. Whitesides, Angew. Chem. Int. Ed. 54 (2015) 3196–3209.
[3] J. Kašpar, P. Fornasiero, N. Hickey, Catal. Today 77 (2003) 419–449.
[4] D. Chatterjee, O. Deutschmann, J. Warnatz, Faraday Discuss. 119 (2001) 371–384.
[5] W. Yang, R. Zhang, B. Chen, D. Duprez, S. Royer, Environ. Sci. Technol. 46 (2012) 11280–11288.
[6] J. Liu, X. Li, Q. Zhao, C. Hao, D. Zhang, Environ. Sci. Technol. 47 (2013) 4528–4535.
[7] F. Figueras, J.L. Flores, G. Delahay, A. Bourane, J.-M. Clacens, A. Desmartin-Chomel, B. Coq, A. Giroir-Fendler, Top. Catal. 39 (2006) 59–64.
[8] F. Poignant, J. Saussey, J.C. Lavalley, G. Mabilon, J. Chem. Soc. Chem. Commun. (1995) 89–90.
[9] L. Capek, K. Novoveska, Z. Sobalık, B. Wichterlova, L. Cider, E. Jobson, Appl. Catal. B 60 (2005) 201–210.
[10] A. Flura, X. Courtois, F. Can, S. Royer, D. Duprez, Top. Catal. 56 (2013) 94–103.
[11] P. Forzatti, I. Nova, E. Tronconi, Angew. Chem. Int. Ed. 48 (2009) 8366–8368.
[12] M. Koebel, M. Elsener, G. Madia, Ind. Eng. Chem. Res. 40 (2001) 52–59.
[13] A. Grossale, I. Nova, E. Tronconi, D. Chatterjee, M. Weibel, Top. Catal. 52 (2009) 1837–1841.
[14] I. Nova, C. Ciardelli, E. Tronconi, D. Chatterjee, B. Bandl-Konrad, Catal. Today 114 (2006) 3–12.
[15] Y.H. Yeom, J. Henao, M.J. Li, W.M.H. Sachtler, E. Weitz, J. Catal. 231 (2005) 181–193.
[16] Y.H. Yeom, B. Wen, W.M.H. Sachtler, E. Weitz, J. Phys. Chem. B 108 (2004) 5386–5392.
[17] M. Li, J. Henao, Y. Yeom, E. Weitz, W.M.H. Sachtler, Catal. Lett. 98 (2004) 5–9.
[18] M. Li, Y. Yeom, E. Weitz, W.M.H. Sachtler, Catal. Lett. 112 (2006) 129–132.
[19] Y.H. Yeom, M. Li, W.M.H. Sachtler, E. Weitz, J. Catal. 246 (2007) 413–427.
[20] I. Nova, E. Tronconi (Eds.), Urea-SCR Technology for DeNOx After Treatment of Diesel Exhausts, Springer, 2014, http://dx.doi.org/10.1007/978-1-4899-8071-7.
[21] A. Flura, F. Can, X. Courtois, S. Royer, D. Duprez, Appl. Catal. B 126 (2012) 275–289.
[22] Y.H. Yeom, M. Li, W.M.H. Sachtler, E. Weitz, J. Catal. 238 (2006) 100–110.
[23] F. Can, A. Flura, X. Courtois, S. Royer, G. Blanchard, P. Marécot, D. Duprez, Catal. Today 164 (2011) 474–479.
[24] Y.F. Tham, J.-Y.C. Chen, R.W. Dibble, Proc. Combust. Inst. 32 (2009) 2827–2833.
[25] S. Kameoka, T. Chafik, Y. Ukisu, T. Miyadera, Catal. Lett. 55 (1998) 211–215.
[26] J. Deng, J. Wang, X. Xu, Catal. Lett. 35 (1995) 75–88.
[27] K. Eränen, F. Klingstedt, K. Arve, L. Lindfors, D.Y. Murzin, J. Catal. 227 (2004) 328–343.
[28] J. Shibata, K. Shimizu, Y. Takada, A. Shichi, H. Yoshida, S. Satokawa, A. Satsuma, T. Hattori, J. Catal. 227 (2004) 367–374.
[29] X. Zhang, H. He, Z. Ma, Catal. Commun. 8 (2007) 187–192.
[30] S. Fogel, P. Gabrielsson, Appl. Catal. B 158–159 (2014) 1–10.
[31] K.-I. Shimizu, A. Satsuma, Appl. Catal. B 77 (2007) 202–205.
[32] M. Richter, R. Fricke, R. Eckelt, Catal. Lett. 94 (2004) 115–118.
[33] V. Houel, P. Millington, R. Rajaram, A. Tsolakis, Appl. Catal. B 73 (2007) 203–207.
[34] V. Houel, P. Millington, R. Rajaram, A. Tsolakis, Appl. Catal. B 77 (2007) 29–34.
[35] B. Sawatmongkhon, A. Tsolakis, S. Sitshebo, J. Rodriguez-Fernandez, M. Ahmadinejad, J. Collier, R.R. Rajaram, Appl. Catal. B 97 (2010) 373–380.
[36] T.E. Hoost, R.-J. Kudla, K.M. Collins, M.S. Chattha, Appl. Catal. B 13 (1997) 59–67.
[37] T. Sato, S. Goto, Q. Tang, S. Yin, J. Mater. Sci. 43 (2008) 2247–2253.
[38] N. Apostolescu, B. Geiger, K. Hizbullah, M.T. Jan, S. Kureti, D. Reichert, F. Schott, W. Weisweiler, Appl. Catal. B 62 (2006) 104–114.
[39] G. Qi, R.T. Yang, R. Chang, Appl. Catal. B 51 (2004) 93–106.
[40] F. Can, S. Berland, S. Royer, X. Courtois, D. Duprez, ACS Catal. 3 (2013) 1120–1132.
[41] A. Musi, P. Massiani, D. Brouri, J.M. Trichard, P. Da Costa, Catal. Lett. 128 (2009) 25–30.
[42] V. Vinogradoff, F. Duvernay, M. Farabet, G. Danger, P. Theulé, F. Borget, J.C. Guillemin, T. Chiavassa, J. Phys. Chem. A 116 (2012) 2225–2233.
[43] R. Jin, Y. Liu, Z. Wu, H. Wang, T. Gu, Chemosphere 78 (2010) 1160–1166.
[44] Y. Amenomiya, J. Catal. 46 (1977) 326–339.
[45] M. Amblard, R. Burch, B.W.L. Southward, Catal. Today 59 (2000) 365–371.
[46] J.B. Peri, J. Phys. Chem. 69 (1965) 231–239.
[47] K.-I. Shimizu, H. Kawabata, A. Satsuma, T. Hattori, J. Phys. Chem. B 103 (1999) 5240–5245.
[48] T. Venkov, K. Hadjiivanov, D. Klissurki, Phys. Chem. Chem. Phys. 4 (2002) 2443–2448.
[49] G.M. Underwood, T.M. Miller, V.H. Grassian, J. Phys. Chem. A 103 (1999) 6184–6190.
[50] C. Börensen, U. Kirchner, V. Scheer, R. Vogt, R. Zellner, J. Phys. Chem. A 104 (2000) 5036–5045.
[51] Y. Yu, H. He, Q. Feng, H. Gao, X. Yang, Appl. Catal. B 49 (2004) 159–171.
[52] S. Tamm, N. Vallim, M. Skoglundh, L. Olsson, J. Catal. 307 (2013) 153–161.
[53] A.A. Tsyganenko, V.N. Filimonov, Spectrosc. Lett. 5 (1972) 477–487.
[54] A.A. Tsyganenko, V.N. Filimonov, J. Mol. Struct. 19 (1973) 579–589.
[55] H. Knözinger, P. Ratnasamy, Catal. Rev. Sci. Eng. 17 (1978) 31–70.
[56] W. El-Nadjar, M. Bonne, E. Trela, L. Rouleau, A. Mino, S. Hocine, E. Payen, C. Lancelot, C. Lamonier, P. Blanchard, X. Courtois, F. Can, D. Duprez, S. Roer, Microporous Mesoporous Mater. 158 (2012) 88–98.
[57] H. Idriss, Platin. Met. Rev. 48 (2004) 105–115.

[58] K. Eränen, F. Klingstedt, K. Arve, L. Lindfors, D.Y. Murzin, J. Catal. 227 (2004) 328–343.
[59] J. Shibata, K. Shimizu, Y. Takada, A. Shichi, H. Yoshida, S. Satokawa, A. Satsuma, T. Hattori, J. Catal. 227 (2004) 367–374.
[60] A.Y. Stakheev, P.V. Pributkov, S. Dahl, I. Gekas, G.N. Baeva, G.O. Bragina, N.S. Telegina, Top. Catal. 52 (2009) 1821–1825.
[61] J.F. DeWilde, C.J. Czopinski, A. Bhan, ACS Catal. 4 (2014) 4425–4433.
[62] D.E. Doronkin, S. Fogel, S. Tamm, L. Olsson, T. Khan, T. Bligaard, P. Gabrielsson, S. Dahl, Appl. Catal. B 113–114 (2012) 228–236.
[63] Y. Yeom, M. Li, A. Savara, W. Sachtler, E. Weitz, Catal. Today 136 (2008) 55–63.
[64] M. Seneque, X. Courtois, F. Can, D. Duprez, Top. Catal. 59 (2016) 938–944.